Applied Catalysis B: Environmental 192 (2016) 116–125

Contents lists available at ScienceDirect

Applied Catalysis B: Environmental

journal homepage: www.elsevier.com/locate/apcatb

A facile synthesis of Br-modified g-C_3N_4 semiconductors for photoredox water splitting

Zhi-An Lan, Guigang Zhang, Xinchen Wang*

State Key Laboratory of Photocatalysis on Energy and Environment, College of Chemistry, Fuzhou University, Fuzhou 350002, China

ARTICLE INFO

Article history:
Received 22 January 2016
Received in revised form 24 March 2016
Accepted 26 March 2016
Available online 26 March 2016

Keywords:
Photocatalysis
Water splitting
Bromine
Graphitic carbon nitride
Doping

ABSTRACT

Hydrogen production by semiconductor photocatalysis using abundant sunlight and water is an ideal method to address the globe energy and environment issues. Here, we present a facile synthesis of bromine doped graphitic carbon nitride (g-C_3N_4) photocatalysts for hydrogen evolution with visible light irradiation. Bromine modification is shown to enhance the optical, conductive and photocatalytic properties of g-C_3N_4, while still keeping the poly-tri-s(triazine) core structure as the main building blocks of the materials. This modification method can be generally applicable to several precursors of g-C_3N_4, including urea, dicyandiamide, ammonium thiocyanide, and thiourea. The optimal sample CNU-$Br_{0.1}$ shows more than two times higher H_2 evolution rates than pure CNU sample under visible light irradiation, with high stability during the prolonged photocatalytic operation. Results also found that the photocatalytic O_2 evolution activity of CNU-$Br_{0.1}$ was promoted when the sample was subjected to surface kinetic promotion by loading with cobalt oxide as a cocatalyst. This study affords us a feasible modification pathway to rationally design and synthesize g-C_3N_4 based photocatalysts for a variety of advanced applications, including CO_2 photofixation, organic photosynthesis and environmental remediation.

1. Introduction

Energy and environment problems associated with the increasing assumption of fossil resources have limited the sustainable development of human society. This calls for the search for renewable energy resources alternative to fossil fuels. Among the numerous energy carriers, hydrogen is one of the ideal alternative candidates that can be used to generate electricity in H_2-O_2 fuel cells, with water as the only products, being a carbon-neutral energy cycle. Water is abundant on the Earth and it contains 11.1% hydrogen in weight. Therefore, the most promising and simplest approach for hydrogen production is to liberate hydrogen from water by semiconductor photocatalysis using sunlight, by which solar energy is converted and stored in the chemical bond of dihydrogen molecules.

Since the pioneer report by Fujishima and Honda in 1972 that water can be photoelectrochemically decomposed into its constituted elements by Pt and rutile-TiO_2 electrodes with light irradiation, hydrogen production via photocatalytic water splitting has been considered as an ideal pathway to convert the diffused solar energy into intense chemical energy in the form of chemical bonds in energized chemicals, such as H_2 and O_2 [1]. During the past 40 years, many studies have been focused on the rational design and synthesis of inorganic semiconductors with high quantum efficiency and/or broad optical absorption in visible spectrum for photocatalytic water splitting. Among these materials, TiO_2 is the most widely investigated photocatalyst that however in its pristine form is limited by its inherent large band gap energy of 3.2 eV, only excitable with UV-light that occupies less than 5% of the solar spectrum [2]. This has motivated intensive research activities on the modification of TiO_2 with surface defects or dopants [3]. Concurrently, non-TiO_2 based semiconductors as sunlight harvesters has also been actively investigated, such as metal (oxy) sulfides and metal (oxy) nitrides including MoS_2 [4], $NaTaO_3$ [5], ZnGaON [6]. The implication of these photocatalyts for water splitting required the kinetic controls using co-catalysts to reduce reaction barrier and to improve reaction rate.

The development of new visible light photocatalysts has very recently experienced an extension from inorganic semiconductors to solid polymer/organic semiconductors featuring conjugated structures with many unique properties, including tunable band structures, ease processibility, and controllable surface heterostructure. A typical case of such conjugated photocatalyts is the emerged graphitic carbon nitride (g-C_3N_4) polymer that has

* Corresponding author.
E-mail address: xcwang@fzu.edu.cn (X. Wang).

http://dx.doi.org/10.1016/j.apcatb.2016.03.062
0926-3373/

been demonstrated to be able to catalyze photoredox reactions, like water splitting, CO_2 reduction, organic synthesis, and the mineralization of phenolic compounds [7–10]. However, it is recognized that melon-based g-C_3N_4 has been limited by its marginal optical absorption in the visible, high exciton binding energy, low charge migration rate. [11]. A series of strategies were therefore developed to modify g-C_3N_4, for example by nanostructure engineering [12–14], copolymerization [15,16], crystal-structure engineering [17–19], heterostructure construction [20–23]. Doping treatment of g-C_3N_4 has also been regarded as an effective approach to overcome the issues by maximizing its full potential for solar applications [24].

Doping, a process of incorporating external impurities into a semiconductor, is a traditional modification strategy to modulate the bulk and surface electronic structure of semiconductors for the manipulation of conductive, optical, luminescent, magnetic, or other physical properties [25]. In photocatalysis, band-gap engineering through hole- (p-type) or electron- (n-type) doping has been demonstrated as an effective procedure to modify inorganic semiconductor photocatalysts for solar energy applications. A successful case of such a doping treatment of photocatalysts is the doping of Zn into GaN, which has been demonstrated to induce 3d-2p orbital hybridization of Zn and N atoms to narrow the band gap energy of GaN for photocatalytic water splitting [6]. Doping is also widely used to optimize the conductivity of a polymeric material. For instance, after doping with iodine, the charge conductivity of polyacetylene can be increased from $10^{-3}\ \Omega^{-1}\ cm^{-1}$ to $10\ \Omega^{-1}\ cm^{-1}$ [26], enabling its transfer from semiconductor regime to metallic regime that can be widely developed in such fields as solar cells, transistor, etc. Such a material engineering strategy can also be introduced for the modification of g-C_3N_4 polymer photocatalysts. When g-C_3N_4 polymers were modified with non-metal elements, such as B [27], S [28–30], and P [31–34], the electronic and optical properties were efficiently optimized to promote photocatalytic performance due to the enhanced optical absorption and accelerated charge mobility. We therefore believe that efficient g-C_3N_4 photocatalysts can be rationally designed and synthesized by modification on the chemical compositions and nanostructures.

F and I have been applied to dope g-C_3N_4. In the literature survey on these investigations, it was found that fluorine dopant gave much less promotional effect on the optical absorption of g-C_3N_4 than iodine. [35,36]. This is because the valence electrons in the iodine atom with much less electronegativity (F:3.98, I:2.66) are more delocalized/mobile to interact with the pi-electron system of g-C_3N_4. Such an extended conjugation system gives rise to the red-shift of the optical absorption of g-C_3N_4. However, the overlarge size of iodine atom is thermodynamically and geometrically difficult to substitute the nitrogen atom in the tri-s-triazine unites to form stable structure, which somewhat counteracts the beneficial effect of the doping treatment. To this end, bromine in the middle of F and I is a recommended choice to modify g-C_3N_4.

In the previous study, bromine has been doped into many kinds of materials. For example, the intrinsic material performance of polycrystalline $In_4Se_{2.5}$ and graphene have been remarkably improved after the doping treatment with bromine [37,38]. The impact of bromine doping on the photophysical properties of a homodinuclear Ru–tpphz–Ru photosensitizer was also reported by Kuhnt et al. [39]. In photocatalysis, Gao's research shown that the doping of bromine into TiO_2:Sm^{3+} could enhance its photocatalytic performances [40]. According to these reports, bromine is much likely to be the suitable modifier for g-C_3N_4 to tune its physical and chemical properties. Our previous study indeed showed that Br-modification can enhance photocatalytic activity of g-C_3N_4, but the synthesis has not been optimized.

In this article, we developed a facile co-condensation strategy to obtain Br-modified g-C_3N_4 by using urea and ammonia bromine as the starting materials. For a further optimization study, we have performed the synthesis by using other g-C_3N_4 precursors, such as thiourea, dicyandiamide, and ammonium thiocyanide, to react with ammonia bromine to produce Br-doped g-C_3N_4. The study was also performed on the optimization in the doping amount and the synthetic conditions in details, including reaction temperature and reaction time. The as-obtained bromine modified g-C_3N_4 (here, named as CN-Br for simplicity) was applied for photocatalytic hydrogen evolution reaction under visible light irradiation. Results demonstrated that the photocatalytic activity of CN-Br can be efficiently promoted by the introduction of bromine dopants. The specific impact of the bromine modification on the physical and photocatalytic performance of CN-Br was also discussed on the basis of various physical characterization results.

2. Experimental

2.1. Preparation of samples

All the chemicals were used as received without further purification.

2.1.1. Synthesis of g-C_3N_4

In a typical synthesis, 10 g of urea was calcined at 550 °C in air for 2 h at a heating rate of 5.0 °C min^{-1}. The obtained g-C_3N_4 sample was denoted as CNU. Other precursors (dicyandiamide, ammonium thiocyanide, thiourea) were also used to synthesize g-C_3N_4 sample by the similar method, and the resultant samples were denoted as CND, CNA, and CNT, respectively.

2.1.2. Synthesis of CN-Br

The bromine modified CNU samples were prepared by mixing urea (10 g) with different amounts of NH_4Br in 10 mL deionized water with stirring at 80 °C to remove water. The resultant solids were sintered at 550 °C for 2 h with a heating rate 5.0 °C min^{-1} in air. The final samples were denoted as CNU-Br_x, where x represents to the initial amount of bromide amonium (x = 0.01, 0.05, 0.1, 0.3, and 0.5 g) for the ease reproducibility of the synthesis by others. The bromine modified CND, CNA, and CNT were synthesized by the similar method by using the corresponding precursors and 0.1 g NH_4Br, and the as-prepared samples were named as CND-Br, CNA-Br, CNT-Br, respectively.

2.1.3. Synthesis of cobalt deposited CNU-Br

0.2 g CNU-Br solids were immersed in an aqueous solution containing 1.8 mg $Co(NO_3)_2$ (0.3 wt.% as Co). After evaporation with water vapor, the as-prepared mixture was calcined at 300 °C for 1 h in the air. The final solids were denoted as CoO_x/CNU-Br for simplicity.

2.2. Characterization

Powder X-ray diffraction (XRD) measurements were performed on a Bruker D8 Advance diffractometer with Cu-Kα1 radiation (λ = 1.5406 Å). The accelerating voltage and the applied current were 40 kV and 40 mA, respectively. Data were recorded at a scan rate of 0.02° 2θ s^{-1} in the 2θ range from 5° to 60°. Fourier transform infrared (FTIR) spectra were recorded on a BioRad FTS 6000 spectrometer, and the samples were prepared as KBr pellets. Raman spectra were recorded on a HR 800 system, HORIBA Jobin Yvon, and employed for the analysis of the chemical structure of the catalyst. The UV/vis picture was recorded on a Cary 500 Scan Spectrophotometer (Varian, USA). X-ray photoelectron spectroscopy (XPS) data were obtained on a Thermo ESCALAB250 instrument with a monochromatized Al Kα line source (200 W). Nitrogen

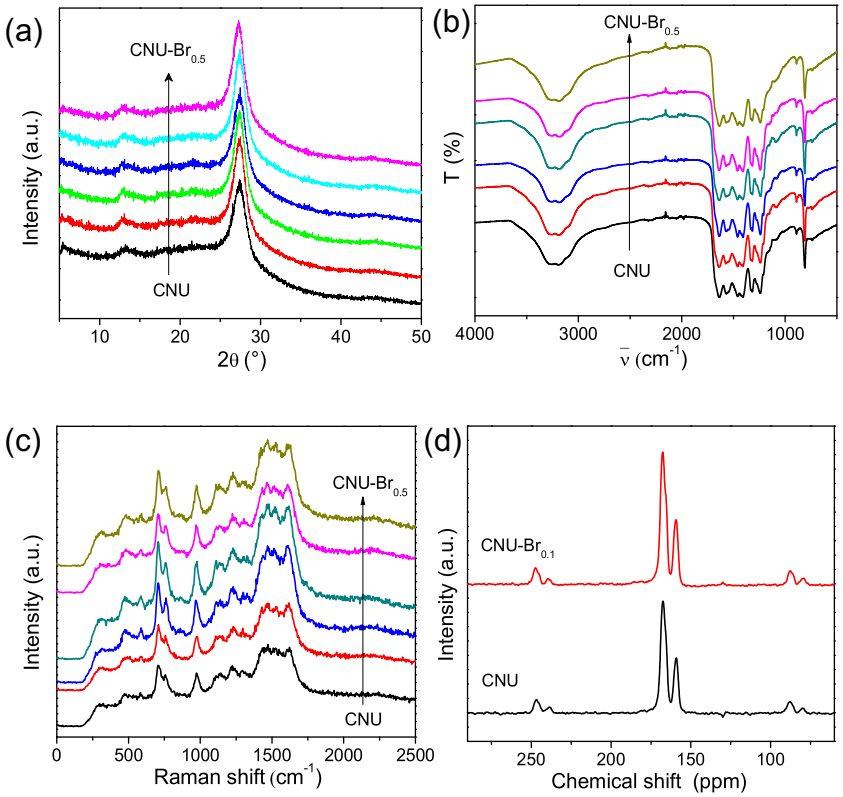

Fig. 1. Power-XRD patterns (a), FT-IR spectra (b) and UV-Raman spectra (c) solid state ^{13}C NMR spectra (d) of CNU and CNU-Br_x samples.

adsorption–desorption isotherms were collected at a Micromeritics ASAP 2020 surface area and porosity analyzer. The sample was degassed at 413 K for 5 h and then analyzed at 77 K. The relative pressure (P/P_0) range used for calculation of BET surface area was from 0.05 to 0.35. The scanning emission microscope (SEM) measurements were conducted using a FEI Nova NanoSEM 230 Field Emission Scanning Electron Microscope. Transmission electron microscopy (TEM) image was recorded using a JEOL Model JEM 2010 EX instrument at an accelerating voltage of 200 kV. UV–vis diffuse reflectance spectra (DRS) were performed on a Varian Cary 500 Scan UV–vis system. $BaSO_4$ was used as a reflectance standard. The optical properties were evaluated by F(R), and they were applied with a Kubelka-Munk correction. Photoluminescence spectra were recorded on an Edinburgh FI/FSTCSPC 920 spectrophotometer under the excitation wavelength of 400 nm at room temperature. Electron paramagnetic resonance (EPR) measurements were carried out on a Bruker model A300 spectrometer. The settings for the EPR spectrometer were as follows: center field, 3510.00 G; microwave frequency, 9.79 GHz; power, 5.05 mW. Electrochemical measurements were conducted with a BAS Epsilon Electrochemical System in a conventional three electrode cell, using a Pt plate as the counter electrode and an Ag/AgCl electrode (3 M KCl) as the reference electrode, the active area is confined to 0.25 cm^2. The electrolyte was 0.2 M Na_2SO_4 aqueous solution without additive (pH 6.8). The working electrode was prepared on indium-tin oxide (ITO) glass that was cleaned by sonication in ethanol for 30 min and dried at 353 K. The boundary of ITO glass was protected using Scotch tape. The 5 mg sample was dispersed in 1 mL of DMF by sonication to get a slurry. The slurry was spread onto pretreated ITO glass. After air-drying, the working electrode was further dried at 393 K for 2 h to improve adhesion. Then, the Scotch tape was unstuck, and the uncoated part of the electrode was isolated with epoxy resin.

2.3. Photocatalytic test

2.3.1. Hydrogen evolution

Photocatalytic hydrogen evolution reactions were performed in a top-irradiation type vessel linked to a glass closed gas system. H_2 production was carried out by dispersing 50 mg photocatalyst powder in an aqueous solution (100 mL) containing triethanolamine (10 vol.%) as sacrificial electron donor. 3.0 wt.% Pt was loaded on the surface of photocatalyst by the in-situ photodeposition approach using H_2PtCl_6. The mixture was evacuated several times to remove air completely before irradiation under a 300 W Xe-lamp equipped with an appropriate long pass cut-off filter, and a water-cooling filter to keep the reaction temperature at ca. 12 °C. The generated gases were analyzed by gas chromatography equipped with a thermal conductive detector (TCD). Argon was used as the carrier gas of the gas chromatography.

2.3.2. Oxygen evolution

Photocatalytic oxygen evolution was carried out in a top-irradiation type reaction vessel connected to a glass closed gas circulation system. For each reaction, 50 mg catalyst powder was well dispersed in an aqueous solution (100 mL) containing $AgNO_3$ (0.01 M) as an electron acceptor and La_2O_3 (0.2 g) as a pH buffer agent. The mixture was evacuated several times to remove air completely before irradiation under a 300 W Xe-lamp. The visible light illumination was provided by placing an appropriate long pass cut-off filter in the front of the Xe lamp. The temperature of the reaction solution was kept at 12 °C by a flow of cooling water. The generated gases were analyzed by gas chromatography equipped with a thermal conductive detector (TCD). Argon was used as the carrier gas of the gas chromatography.

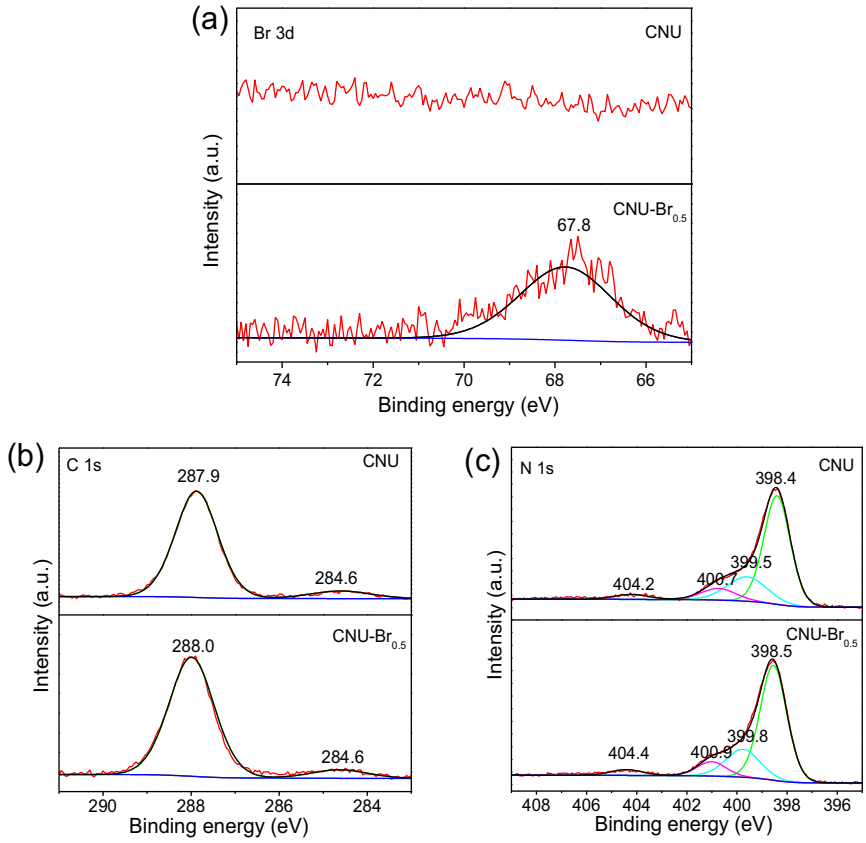

Fig. 2. Br 3d (a), C 1s (b), N 1s (c) high-resolution XPS spectra of CNU and CNU-Br samples.

3. Results and discussion

The crystal structure, texture, optical and electronic properties of the as-prepared CNU-Br_x polymers were carefully investigated by various characterization methods. In the first place, XRD, FT-IR, UV- Raman, and solid state ^{13}C NMR measurements were carried out to determine the crystal and chemical structure of the as-prepared CNU and CNU-Br_x polymers. As shown in Fig. 1a, both pure CNU and CNU-Br_x samples presented similar XRD patterns, which is an indication of the successful fabrication of graphitic-like carbon nitride phase by the thermal-induced condensation reaction using urea as the precursor. Evidently, two distinct XRD peaks at $2\theta = 13.0^\circ$ and 27.4° were observed for all the samples, which were assigned to the (100) and (002) plane of the typical graphitic layer structures [41]. The peak at 13.0° was related to the in-plane repeating units of the heptizine heteroatom cycles, while the later one was assisgned to the graphitic layer stacking, similar in graphite. Interestingly, there is not noticeable change in the chemical skeleton and crystal structure of the sample after the modification, even when the initial amounts of NH_4Br were as high as 0.5 g. To further investigate the structure of the as-prepared polymers, FT-IR spectra of the sample was analyzed. In Fig. 1b, it was clear to observe that both pure CNU and CNU-Br_x polymers exhibited similar FT-IR vibration modes. The peaks at 810 cm^{-1} and 1200–1600 cm^{-1} were due to the characteristic breathing and stretching vibration modes of aromatic CN heterocycles, confirming the formation of triazine units. The broad and weak bands at 2900–3300 cm^{-1} were typical signals of N—H or O—H vibrations, which were contributed to the uncondensed amino groups as the surface terminal groups and the absorbed H_2O molecules.

UV-Raman and NMR measurements were also carried out to check the chemical structure of the as-prepared samples (Fig. 1c). The two wide peaks at ~1500 cm^{-1} are attributed to the D and G bands of a typical graphitic structure [42], once again confirming the derivation of graphitic structure. The Raman shifts at 500–1300 cm^{-1} were related to the typical heptazine units. In detail, the two peaks at 709 and 762 cm^{-1} were resulted from the in-plane bending vibrations of the heptazine linkages, while the sharp peaks at 978 cm^{-1} were ascribed from the symmetric N-breathing mode of heptazine units. However, no peaks were energed in the region of 2000–2500 cm^{-1}, indicating the absence of any C=N units or N=C=N linking groups within the carbon nitride framwork. In addition, both samples showed two distinct peaks in the solid state ^{13}C NMR spectra (Fig. 1d). The stronger peak at $\delta \approx 167.4$ ppm was related to the sp^2 hybridized C in the form of N—C=N, while the smaller peak at $\delta \approx 158.8$ ppm was attributed to the C atoms like CN_3 in the melem structure. No new peak could be viewed in the spectra, indicating the robust stability of the heptizine carbon ntiride cycles after engineering with bromine. Therefore, we could conclude that no evident structure change was generated after the doping modification, which was very important to maintain the classical semiconductor properties of graphitic carbon nitride thus to promote photocatalytic applications.

High resolution XPS characterization was carried out to study the surface chemical composition and oxidation state of the elements in the CNU and CNU-Br samples. In Fig. 2a, an obvious single peak at 67.8 eV was observed for CNU-$Br_{0.5}$, which was related to the Br^-, illustrating the presence of bromine species. As expected, CNU and CNU-$Br_{0.5}$ showed similar high resolution C 1s and N 1s core-level XPS spectra. In Fig. 2b, the weak peak at ~284.6 eV was attributed to the sp^2-hybridized carbon in the form of C—C, which was determined as standard carbon. The strong peak at binding energy of ~287.9 eV was assigned to the sp^2-bonded carbon atoms in the heterocycle (N—C=N) of aromatic g-C_3N_4, which was related

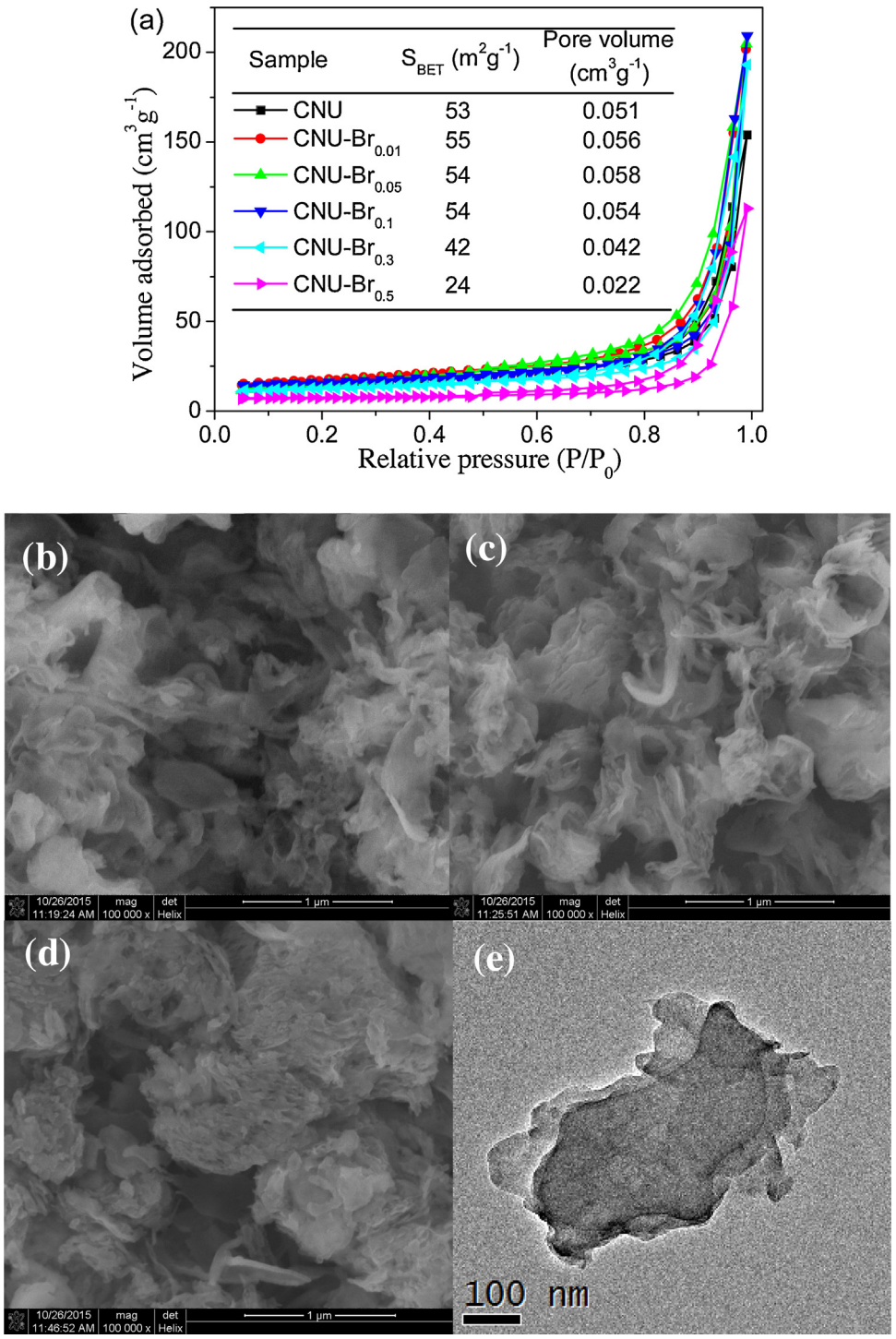

Fig. 3. Nitrogen adsorption-desorption isotherms of CNU and CNU-Br_x samples (a) SEM images of CNU, CNU-$Br_{0.1}$ and CNU-$Br_{0.5}$ samples (b–d); TEM image of CNU-$Br_{0.1}$ sample (e).

to the major skeleton carbon in the triazine-based heterocycle [43]. In Fig. 2c, the high resolution of N 1s spectra could be deconvoluted into four peaks at ~398.4, 399.5, 400.7 and 404.2 eV, respectively. These peaks were corresponded to the sp^2 bonded nitrogen in the form of C—N=C, the tertiary nitrogen (N—$(C)_3$) groups, the surface uncondensed amino groups (C—N—H), and the charging effects or positive charge localization in the heterocycles, respectively [43]. The first two nitrogen together with the sp^2-bonded carbon (N—C=N) make up the triazine-based heterocyclic ring (C_6N_7) units. To analyze the texture and morphology of the as-prepared samples, some characterizations including N_2 adsorption-desorption isotherms, SEM and TEM were performed. It can be seen from Fig. 3a that all the samples exhibit type H1 hysteresis loops, which demonstrates the presence of mesoporous structure [8]. When the adding amounts of NH_4Br are below 0.1 g, the samples show similar BET surface area (ca. 54 $m^2\ g^{-1}$) and pore volume. However, when the amounts of NH_4Br increased to 0.3 or 0.5 g, the BET surface area and pore volume of the sample sharply decreased. This is because the excess introduction of NH_4Br into the urea-condensation reaction may change the texture and the surface morphology of the

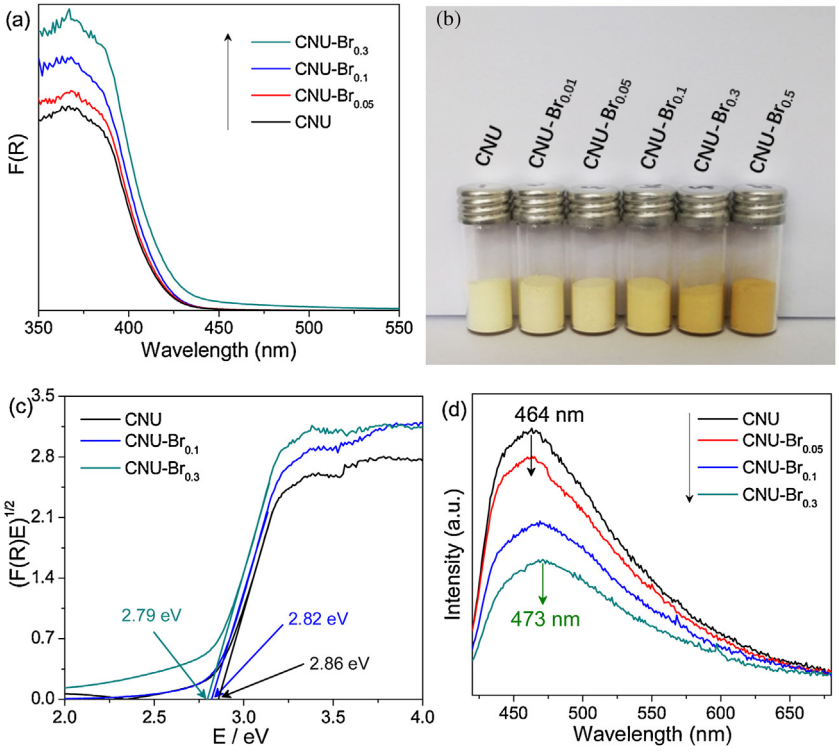

Fig. 4. UV–vis DRS spectra (a), exact appearance (b), bandgap energy (c) and room-temperature PL (d) of CNU and CNU-Br_x samples.

sample, e.g., collapse of mesopores, and thus decrease the surface area (ca. 24 $m^2 g^{-1}$). This morphology change could also be observed in the SEM images. As shown in Fig. 3b and c, the SEM images of CNU and CNU-$Br_{0.1}$ samples exhibit similar typical layered platelet-like (which can be seen in the TEM image in Fig. 3e) and curl-like thin nanosheet. However, as shown in Fig. 3d, when the adding amount of NH_4Br increased to 0.5 g, densely stacked graphitic layer with increased thickness of the nanosheet and the big particle size was obtained, leading to the decrease in the surface area and the pore volume. The obvious change of the surface morphology may be ascribed to the restrained polymerization rate of g-C_3N_4, owing to the formation of NH_3 from the decomposition of NH_4Br at 550 °C. When excess amounts of NH_4Br were added to co-condensation with urea (which involves the release of ammonia gas during the process), the produced NH_3 would impede the intrinsic deamination kinetics, and thus result in the densely stacked graphitic layer. Evidently, the decrease in the surface area and increase in the particle size could result in the low photocatalytic activities. Thus, the adding contents of the NH_4Br should be carefully optimized.

To gather more insights on the bromide modification on the physicochemical properties of the g-C_3N_4 conjugated polymers, the optical properties of the samples were carefully investigated. Fig. 4a displays the UV–vis DRS spectra of the synthesized CNU and CNU-Br_x samples. From the picture we can see that all samples showed the typical semiconductor adsorption. The sharp absorption band thresholds of the samples were centered at ca. 440 nm due to the excitation of electron from the valence band to the conduction band of the conjugated g-C_3N_4 semiconductors, which were well accordance with the traditional g-C_3N_4 semiconductors [24,44], certifying that the modification with bromine could maintain the intrinsic band structure of graphitic carbon nitride. However, as the amount of bromine increased, a clear red-shift of the optical absorption edge was developed. This phenomenon is very common and widely developed for the doping modifications of semiconductors [35,36]. The introduction of heteroatoms into the framework of semiconductor materials always generate impurity energy levels above the valence band edge of the semiconductor, and thus decreasing the involved transition energy of photoexcited electrons [28]. Evidently, fewer input energy was involved for the excitation of charge carriers, and thus decreasing the optical absorption band gap, which were further confirmed by the color change from pale yellow to the dark brown as the adding amount of NH_4Br increased from 0.01 to 0.5 g (Fig. 4b). Simultaneously, the decreased band gap of the samples was calculated and showed in Fig. 4c. The band gap of pure CNU (Eg = 2.86 eV) was decreased from 2.82 to 2.79 eV as the addition amounts of NH_4Br were increased from 0.1 to 0.3 g. The decrease of the band gap was contributed to the capturing of more visible photons, and potentially benefited for improving the photocatalytic performance, e.g., photocatalytic water splitting for hydrogen and oxygen evolution.

In addition, similar red shift of the optical absorption band can be validated by the room temperature photoluminescence (PL) measurement. As shown in Fig. 4c, when the samples were excited by 400 nm visible light, a broad emission peak at ca. 460 nm appeared. An obvious red-shift of the emission peak from 464 to 473 nm was observed for CNU-$Br_{0.3}$, which further certified the decreased band-gap energy of samples after the Br modifications as shown in Fig. 4b. It could be also observed from the picture that the PL intensities of the emission peaks were greatly decreased when the adding amount of NH_4Br were increased, which could indirectly illustrate that the modifications were effective to suppress the rapid charge carrier recombination. This is because the introduction of heteroatoms into the π-conjugated system of g-C_3N_4 can accelerate the charge carriers transfer rate and thus restrain the recombination of electron and hole [36], which are contributed to improve the photocatalytic activities.

More optical and electronic properties of the optimized samples were examined by room temperature electron paramagnetic resonance (EPR). As shown in Fig. 5a, all samples showed one single Lorentzian line centering at a g value of 2.0034 in dark, being originated from unpaired electrons on π-conjugated

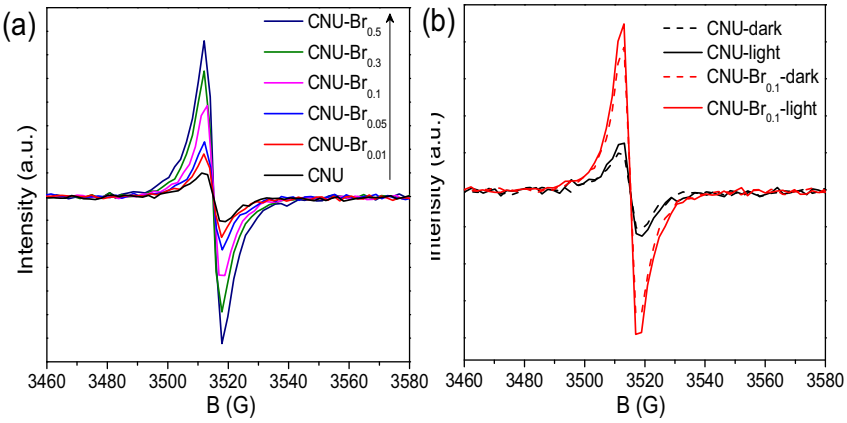

Fig. 5. Room-temperature EPR spectra in dark (a) and under visible light ($\lambda \geq 420$ nm) (b) for the CNU and CNU-Br_x samples.

g-C_3N_4 aromatic rings. In addition, the EPR intensities were greatly strengthened when increasing the initial amounts of ammonium bromine. This certifies that the modification can effectively accelerate the electron mobility in the in the π-conjugated system of g-C_3N_4, potentially due to the delocalization of the valance electron of Br to the g-C_3N_4 conjugation system to widen the band distribution to improve charge migration. In addition, greatly enhanced EPR intensities for both CNU and CNU-$Br_{0.1}$ samples were presented under the visible light irradiation (Fig. 5b), indicating the efficient generation of photochemical radical pairs in the modified polymer semiconductors.

Photoelectrochemical measurements including electrochemical impedance spectra (EIS) in dark and transient photocurrent under visible light irradiation was performed to further study the systems. As shown in Fig. 6a, the Nyquist plots of the CNU and CNU-$Br_{0.1}$ electrode materials cycled in 0.2 M Na_2SO_4 electrolyte showed semicircular at high frequencies. Because the high frequency of the Nyquist plots was corresponded to the charge transfer limiting process and can be attributed to the double layer capacitance (C_{dl}) in parallel with the charge transfer resistance (R_{ct}) at the contact interface between the electrode materials and the electrolyte solution. The semicircular of the Nyquist plots were related to the resistance of the electrodes. It was observed in Fig. 6a that a dramatically decreased EIS semicircular were obtained as compared to the pure CNU after the introduction of bromine into the heterocycle of the polymeric system, indicating that elemental doping could facilitate the interfacial charge transfer/migration. Besides, it could be seen from Fig. 6b that both pristine and modified CNU electrodes showed obvious negative photocurrents under visible light irradiation at an applied potential of −0.2 V (vs. Ag/AgCl, pH 6.8). Additionally, CNU-$Br_{0.1}$ showed larger photocurrent density than the pure CNU electrode, which was benefited from the smaller resistance of the electrode materials after the modification, further indicating the advantage of the modification treatment using the non-metal elements.

Taken the above characterizations and discussions together into consideration, we believed that the Br modification was a useful tool to optimize the texture, optical and electronic properties of the intrinsic CNU polymers. Few crystal structure and chemical composition variations were generated after the modification, but the modification can still promote the optical and photocatalytic properties of the carbon nitride polymer.

The photocatalytic activities of the as-prepared pure CNU and CNU-Br_x samples were evaluated in an assay of H_2 evolution from water in the presence of organic sacrificial agents (TEOA). 3 wt.% Pt was in-situ photodeposited on the surface of the photocatalysts as H_2 evolution co-catalyst to promote the H_2 evolution activities under visible irradiation ($\lambda \geq 420$ nm) [45]. As shown in Fig. 7a, the H_2 evolution rates of the as-prepared CNU-Br_x photocatalysts were strongly depended on the adding amount of NH_4Br. First, small amounts of NH_4Br (0.01 g) could largely enhance the photocatalytic activities. The H_2 evolution rate for CNU was determined as 20 μmol h^{-1}, while the value tested for CNU-$Br_{0.01}$ reached 30 μmol h^{-1}. When the adding amount of NH_4Br were varied from 0.01 to 0.1 g, the H_2 evolution rates of the samples were gradually increased (from 30 to 48 μmol h^{-1}) as a function of the NH_4Br contents. Further enhancing the addition amount of NH_4Br from 0.3 to 0.5 g will lead to the fast decrease in the H_2 evolution rate. However, the H_2 evolution rate for CNU-$Br_{0.5}$ (29 μmol h^{-1}) was still higher than that of the pure CNU polymer (20 μmol h^{-1}), directly certifying the positive improvements of the Br modification in promoting the photocatalytic activities. The optimal activity (48 μmol h^{-1}) obtained for CNU-$Br_{0.1}$ sample was 2.4 times higher than that of the pure CNU sample (20 μmol h^{-1}). This enhanced activity was similar with B modified g-C_3N_4 (CN-B) [27], and larger than that of S (CN-S) [30], and P (CN-P) [34] modified g-C_3N_4, as shown in Fig. 7b.

The stability of the photocatalysts was a concern for the applications of polymer based semiconductors. We therefore carried out a cyclic H_2 evolution test of the optimal CNU-$Br_{0.1}$ sample under a prolonged visible light irradiation ($\lambda \geq 420$ nm) of 20 h. Indeed, after 4 consecutive cycle's reactions, nearly no activity decrease was seen in Fig. 7c, indicating the robust property of the optimized CNU-$Br_{0.1}$ catalyst toward the light and solution contact. The overall amount of the H_2 reached 640 μmol after 4 runs of 20 h continuous reaction, which was corresponded to the turnover number (TON) of 84 (based on Pt atoms). In the next set of experiment, we evaluated the H_2 evolution activities of optimal CNU-$Br_{0.1}$ sample under irradiation using different long-pass cut-off optical filters. As we could see in Fig. 7d, the H_2 evolution activity of CNU-$Br_{0.1}$ sample was strongly depended on the incident wavelength, illustrating that the photocatalytic water reduction reaction process was mainly drive by the incident photons that induces the formation of exciton flux and charge carriers. When the wavelength of the irradiation wavelength was extended to as long as 500 nm, it also showed well activities (9 μmol h^{-1}), which was contributed to promote the solar conversion efficiency. Furthermore, to confirm the physical and chemical stability of CNU-$Br_{0.1}$ sample after photocatalytic reactions, the used CNU-$Br_{0.1}$ sample was further subjected to the characterizations by XRD, FT-IR, and DRS (Fig. 8). Results revealed that there is no obvious change in the crystal and chemical structure of the material.

To further demonstrate the universality of this facile bromine modification method to optimize the optical and electronic

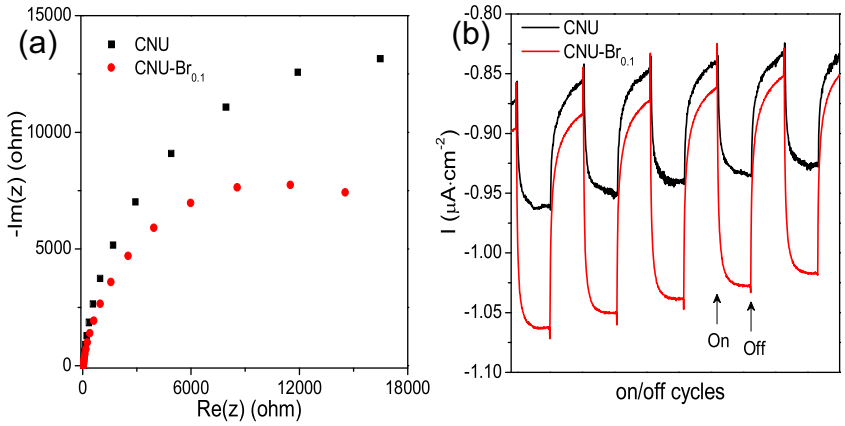

Fig. 6. Electrochemical impedance spectroscopy plots in dark (a) and periodic on/off photocurrent response under visible light irradiation (b) for the CNU and CNU-Br_x samples at a −0.2 V bias potential vs. Ag/AgCl in a 0.2 M Na_2SO_4 aqueous solution (pH = 6.8).

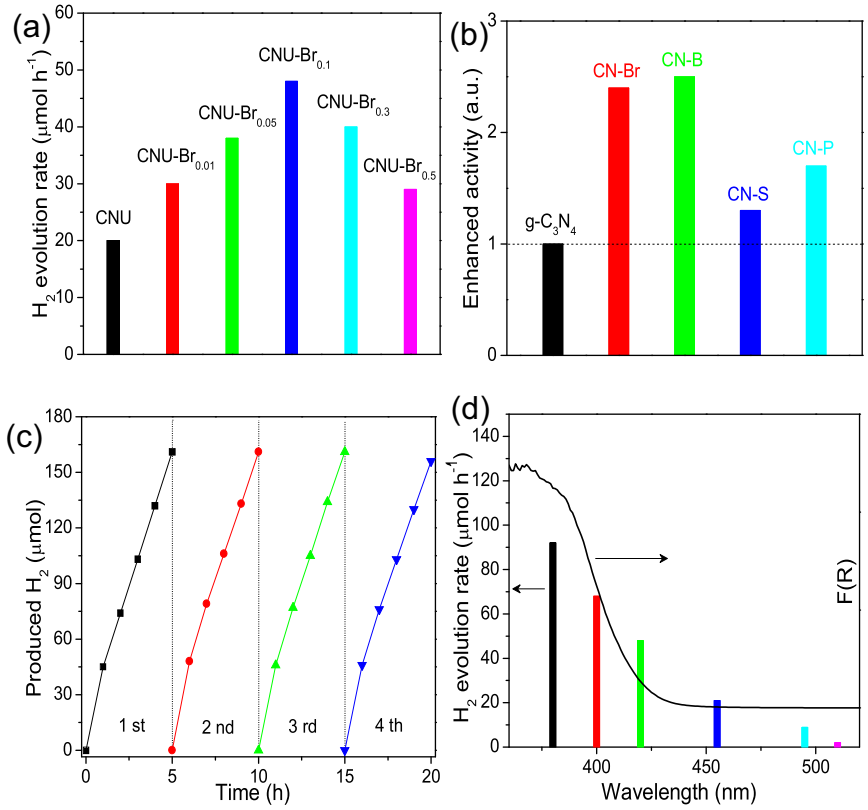

Fig. 7. H_2 evolution rate of CNU modified with different amount of bromine under visible light irradiation (λ ≥ 420 nm) (a); photocatalytic performance for H_2 evolution of pure g-C_3N_4 and different non-metal elements doping g-C_3N_4 (b); Long-term H_2 evolution by CNU-$Br_{0.1}$ under visible light irradiation (λ ≥ 420 nm) (c) and Wavelength dependence of H_2 evolution rate for CNU-$Br_{0.1}$ (d).

properties as well as photocatalytic performance of the pristine g-C_3N_4 polymer, other starting materials, including dicyandiamide, ammonium thiocyanide, thiourea were also selected to prepare bromine modified g-C_3N_4 polymers by using the similar co-condensation approach. The resulting samples were denoted as CND-Br, CNA-Br, and CNT-Br for simplicity, respectively. As shown in Fig. 9, it was clear to observe that all Br-modified samples showed enhanced photocatalytic activities for hydrogen evolution than their pure counterparts under the same photoredox reaction conditions, well elucidating that this bromine modification scheme is indeed general for the optimization of the g-C_3N_4 polymers.

On the basis of the above results, the mechanism for the photocatalytic H_2 production by CN-Br is proposed. As illustrated in Scheme 1, when CN-Br was irradiated by light with energy larger than the band gap, the excited charge was generated, separated and migrated to the surface. When photo-generated charge carriers transferred to the catalyst surface, the electrons reduce protons to generate H_2 while the holes oxidize the TEOA to restrain the charge recombination and promote the photocatalytic activities.

Next, the photocatalytic water oxidation activities for O_2 evolution by the CNU-$Br_{0.1}$ sample were tested. Water oxidation reaction is regarded as a more challenge water half-splitting reaction that involves O—H cleavage and O—O band formation via sluggish 4e transfer pathway. As shown in Fig. 10, the pure CNU-$Br_{0.1}$ sample only shows a limited activity for water oxidation under UV light (4 μmol h^{-1}) or visible light (less than 1 μmol h^{-1})

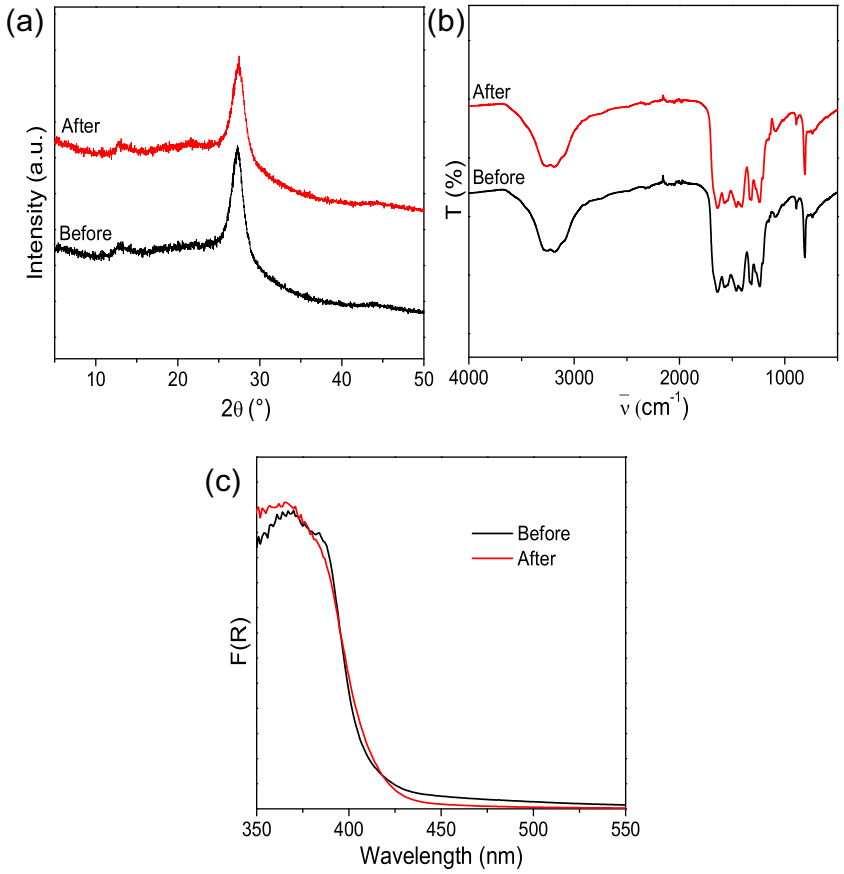

Fig. 8. Power-XRD patterns (a), FT-IR (b), and UV–vis DRS spectra (c) of CNU-$Br_{0.1}$ before and after photoreaction.

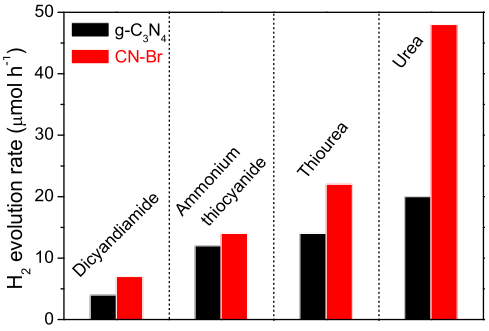

Fig. 9. H_2 evolution rate of CND, CNA, CNT, CNU and their modified samples under visible light irradiation ($\lambda \geq 420$ nm).

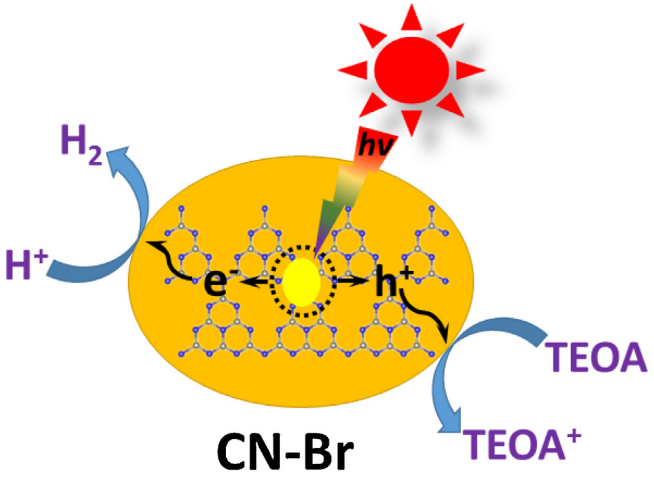

Scheme 1. Proposed reaction mechanism for photocatalytic H_2 evolution on CN-Br.

irradiation. This is because the valence band edge of the CNU-$Br_{0.1}$ is not positive enough to drive the multiple electron/energy transfer process of water oxidation. Besides, the water oxidation reaction was always restrained by the large O_2 evolution over-potential and the sluggish surface kinetics. Particularly, the g-C_3N_4 surface is lack of active sites for catalyzing O_2 evolution reaction. The combination of suitable water oxidation cocatalysts (e.g., cobalt based materials) was generally developed to promote the photocatalytic water oxidation activities of g-C_3N_4- and BCN-based photocatalysts in the previous studies [46–52]. Here, CoO_x was also employed as water oxidation cocatalysts on the surface of CNU-$Br_{0.1}$ to promote the photocatalytic water oxidation activities. As seen in Fig. 8, few amount of CoO_x (0.3 wt.% as Co) deposited on CNU-$Br_{0.1}$ can greatly enhance the water oxidation activities for O_2 evolution under both UV light (23 μmol h^{-1}) and visible light (4 μmol h^{-1}) irradiation. These O_2 evolution rates of CoO_x/CNU-$Br_{0.1}$ were nearly 6 times larger than that of the pure CNU-$Br_{0.1}$. The amount of the O_2 gases were increased when we prolonged the photocatalytic reaction time to 8 h (62 μmol for UV light and 16 μmol for visible light). The slightly decreased evolution rate was mainly due to the reduction of Ag^+ by electrons to deposit metallic Ag nanoparticles on the surface of the CNU-$Br_{0.1}$ photocatalysts which leads to the decrease in the optical absorption ability of the substrate, as usually reported in the previous studies [46–49].

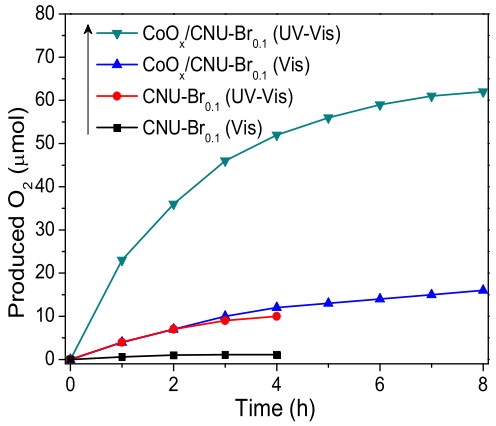

Fig. 10. O_2 evolution by CoO_x/CNU-$Br_{0.1}$ and CNU-$Br_{0.1}$ samples under visible light ($\lambda \geq 420$ nm) or UV–vis light irradiation.

4. Conclusions

In this study, we have developed a series of bromine modified g-C_3N_4 photocatalysts via one-pot co-condensation of urea with NH_4Br. The incorporation of bromine into g-C_3N_4 indeed modulates the texture, optical absorption, conductivity, charge-carrier transfer rate, as well as photocatalytic performance, without destroying the major construction and architecture of the g-C_3N_4 polymer. The optimal CNU-$Br_{0.1}$ sample exhibits improved photocatalytic activity and high photocatalytic stability for H_2 evolution under visible light irradiation. The photocatalytic ability of CNU-$Br_{0.1}$ for water oxidation is also greatly enhanced via loading few amounts of cobalt oxide as water oxidation co-catalyst. This work highlights the importance of bromine modification as a feasible chemical approach to realize the modification of carbon nitride polymers, providing an efficient conjugated semiconductor scaffold for the sustainable solar energy utilization and conversion, e.g., water splitting, CO_2 reduction, and fine chemical production.

Acknowledgments

This work is financially supported by the National Basic Research Program of China (2013CB632405), the National Natural Science Foundation of China (21425309), and the National Key Technologies R & D Program of China (2014BAC13B03).

References

[1] A. Fujishima, K. Honda, Nature 238 (1972) 37–38.
[2] G. Liu, L. Wang, H.G. Yang, H.-M. Cheng, G.Q. Lu, J. Mater. Chem. 20 (2010) 831–843.
[3] J. Schneider, M. Matsuoka, M. Takeuchi, J.L. Zhang, Y. Horiuchi, M. Anpo, D.W. Bahnemann, Chem. Rev. 114 (2014) 9919–9986.
[4] B. Hinnemann, P.G. Moses, J. Bonde, K.P. Jorgensen, J.H. Nielsen, S. Horch, I. Chorkendorff, J.K. Norskov, J. Am. Chem. Soc. 127 (2005) 5308–5309.
[5] H. Kato, K. Asakura, A. Kudo, J. Am. Chem. Soc. 125 (2003) 3082–3089.
[6] K. Maeda, K. Teramura, D.L. Lu, T. Takata, N. Saito, Y. Inoue, K. Domen, Nature 440 (2006) 295.
[7] X.C. Wang, K. Maeda, A. Thomas, K. Takanabe, G. Xin, J.M. Carlsson, K. Domen, M. Antonietti, Nat. Mater. 8 (2009) 76–80.
[8] J. Qin, S. Wang, H. Ren, Y. Hou, X. Wang, Appl. Catal. B: Environ. 179 (2015) 1–8.
[9] Y. Wang, J.S. Zhang, X.C. Wang, M. Antonietti, H.R. Li, Angew. Chem.—Int. Ed. 49 (2010) 3356–3359.
[10] F.F. Liang, Y.F. Zhu, Appl. Catal. B—Environ. 180 (2016) 324–329.
[11] S. Cao, J. Low, J. Yu, M. Jaroniec, Adv. Mater. 27 (2015) 2150–2176.
[12] J.S. Zhang, Y. Chen, X.C. Wang, Energy Environ. Sci. 8 (2015) 3092–3108.
[13] D. Zheng, G. zhang, X. Wang, Appl. Catal. B: Environ. 179 (2015) 479–488.
[14] Y. Zheng, L.H. Lin, X.J. Ye, F.S. Guo, X.C. Wang, Angew. Chem.—Int. Ed. 53 (2014) 11926–11930.
[15] J. Zhang, X. Chen, K. Takanabe, K. Maeda, K. Domen, J.D. Epping, X. Fu, M. Antonietti, X. Wang, Angew. Chem.—Int. Ed. 49 (2010) 441–444.
[16] M.W. Zhang, X.C. Wang, Energy Environ. Sci. 7 (2014) 1902–1906.
[17] Y.-S. Jun, J. Park, S.U. Lee, A. Thomas, W.H. Hong, G.D. Stucky, Angew. Chem.—Int. Ed. 52 (2013) 11083–11087.
[18] G. Algara-Siller, N. Severin, S.Y. Chong, T. Bjorkman, R.G. Palgrave, A. Laybourn, M. Antonietti, Y.Z. Khimyak, A.V. Krasheninnikov, J.P. Rabe, U. Kaiser, A.I. Cooper, A. Thomas, M.J. Bojdys, Angew. Chem.—Int. Ed. 53 (2014) 7450–7455.
[19] E. Wirnhier, M. Doblinger, D. Gunzelmann, J. Senker, B.V. Lotsch, W. Schnick, Chem.—Eur. J. 17 (2011) 3213–3221.
[20] C. Pan, J. Xu, Y. Wang, D. Li, Y. Zhu, Adv. Funct. Mater. 22 (2012) 1518–1524.
[21] Y.D. Hou, A.B. Laursen, J.S. Zhang, G.G. Zhang, Y.S. Zhu, X.C. Wang, S. Dahl, I. Chorkendorff, Angew. Chem.—Int. Ed. 52 (2013) 3621–3625.
[22] J.S. Zhang, M.W. Zhang, R.Q. Sun, X.C. Wang, Angew. Chem.—Int. Ed. 51 (2012) 10145–10149.
[23] Y. Wang, R. Shi, J. Lin, Y. Zhu, Energy Environ. Sci. 4 (2011) 2922–2929.
[24] Y. Zheng, L.H. Lin, B. Wang, X.C. Wang, Angew. Chem.—Int. Ed. 53 (2015) 12868–12884.
[25] S.C. Erwin, L.J. Zu, M.I. Haftel, A.L. Efros, T.A. Kennedy, D.J. Norris, Nature 436 (2005) 91–94.
[26] C.K. Chiang, Y.W. Park, A.J. Heeger, H. Shirakawa, E.J. Louis, A.G. MacDiarmid, J. Chem. Phys. 69 (1978) 5098–5104.
[27] Z.Z. Lin, X.C. Wang, Angew. Chem.—Int. Ed. 52 (2013) 1735–1738.
[28] G. Liu, P. Niu, C. Sun, S.C. Smith, Z. Chen, G.Q. Lu, H.-M. Cheng, J. Am. Chem. Soc. 132 (2010) 11642–11648.
[29] K. Wang, Q. Li, B.S. Liu, B. Cheng, W.K. Ho, J.G. Yu, Appl. Catal. B—Environ. 176 (2015) 44–52.
[30] J. Hong, X. Xia, Y. Wang, R. Xu, J. Mater. Chem. 22 (2012) 15006.
[31] L. Zhang, X. Chen, J. Guan, Y. Jiang, T. Hou, X. Mu, Mater. Res. Bull. 48 (2013) 3485–3491.
[32] J. Ran, T.Y. Ma, G. Gao, X.-W. Du, S.Z. Qiao, Energy Environ. Sci. 8 (2015) 3708–3717.
[33] T.Y. Ma, J. Ran, S. Dai, M. Jaroniec, S.Z. Qiao, Angew. Chem.—Int. Ed. 54 (2015) 4646–4650.
[34] S. Guo, Z. Deng, M. Li, B. Jiang, C. Tian, Q. Pan, H. Fu, Angew. Chem. 55 (2016) 1830–1834.
[35] Y. Wang, Y. Di, M. Antonietti, H.R. Li, X.F. Chen, X.C. Wang, Chem. Mat. 22 (2010) 5119–5121.
[36] G.G. Zhang, M.W. Zhang, X.X. Ye, X.Q. Qiu, S. Lin, X.C. Wang, Adv. Mater. 26 (2014) 805–809.
[37] Y. Luo, J. Yang, G. Li, M. Liu, Y. Xiao, L. Fu, W. Li, P. Zhu, J. Peng, S. Gao, J. Zhang, Adv. Energy Mater. 4 (2014) 1300599.
[38] K. Ueno, R. Kosugi, K. Imazeki, A. Aozasa, Y. Matsumoto, H. Miyazaki, N. Sakuma, A. Kajita, T. Sakai, Jpn. J. Appl. Phys. 53 (2014) 05GC02.
[39] C. Kuhnt, M. Karnahl, S. Rau, M. Schmitt, B. Dietzek, J. Popp, Chem. Phys. Lett. 516 (2011) 45–50.
[40] C.M. Gao, H.W. Song, L.Y. Hu, G.H. Pan, R.F. Qin, F. Wang, Q.L. Dai, L.B. Fan, L.N. Liu, H.H. Liu, J. Lumines 128 (2008) 559–564.
[41] A. Thomas, A. Fischer, F. Goettmann, M. Antonietti, J.O. Muller, R. Schlogl, J.M. Carlsson, J. Mater. Chem. 18 (2008) 4893–4908.
[42] G. Zhang, G. Li, X. Wang, ChemCatChem 7 (2015) 2864–2870.
[43] J. Liu, T. Zhang, Z. Wang, G. Dawson, W. Chen, J. Mater. Chem. 21 (2011) 14398–14401.
[44] Y.D. Hou, Y.S. Zhu, Y. Xu, X.C. Wang, Appl. Catal. B—Environ. 156 (2014) 122–127.
[45] Y. Zheng, Z.M. Pan, X.C. Wang, Chin. J. Catal. 34 (2013) 524–535.
[46] G. Zhang, S. Zang, X. Wang, ACS Catal. 5 (2015) 941–947.
[47] G. Zhang, S. Zang, Z.-A. Lan, C. Huang, G. Li, X. Wang, J. Mater. Chem. A 3 (2015) 17946–17950.
[48] G. Zhang, C. Huang, X. Wang, Small (Weinheim an der Bergstrasse Germany) 11 (2015) 1215–1221.
[49] M. Zhang, Z. Luo, M. Zhou, C. Huang, X. Wang, Sci. China Mater. 58 (2015) 867–876.
[50] C. Huang, C. Chen, M. Zhang, L. Lin, X. Ye, S. Lin, M. Antonietti, X. Wang, Nat. Commun. 6 (2015) 7698–7704.
[51] G. Zhang, Z.-A. Lan, L. Lin, S. Lin, X. Wang, Chem. Sci. (2016), http://dx.doi.org/10.1039/c5sc04572j.
[52] G. Zhang, S. Zang, L. Lin, Z.-A. Lan, G. Li, X. Wang, ACS Appl. Mater. Interfaces 8 (2016) 2287–2296.